Supplementary Information for "Inverse catalysts: Tuning the composition and structure of oxide clusters through the metal support"

Luuk H. E. Kempen[1] and Mie Andersen[1,2,*]

[1]Center for Interstellar Catalysis, Department of Physics and Astronomy, Aarhus University, Aarhus C, Denmark
[2]Aarhus Institute of Advanced Studies, Aarhus University, Aarhus C, Denmark
[*]Corresponding author: mie@phys.au.dk

S1 Gas-phase DFT error correction

The PBE functional does not accurately reproduce experimental gas-phase reaction enthalpies. Using a procedure of correlating reaction enthalpies with different functionals [1], an earlier analysis of systematic errors shows that especially multiply-bonded molecules are most impacted by DFT error [2]. Following the approach of this latter analysis, we determine a correction term applied to the enthalpies of the isolated gas-phase molecules, such that they are evaluated as

$$E_i = E_i^{\mathrm{DFT}} + E_i^{\mathrm{ZPE}} + \varepsilon_i, \tag{S1}$$

where E_i^{DFT} is the DFT-calculated energy of the gas-phase species i, E_i^{ZPE} is the zero-point energy correction, and ε_i is the correction term.

This correction term is chosen such that experimental reaction enthalpies at 0 K are reproduced. The error between reaction enthalpies is defined as

$$\varepsilon = \Delta H_{\mathrm{r}}^{\mathrm{exp}} - \Delta H_{\mathrm{r}}^{\mathrm{DFT}}, \tag{S2}$$

where experimental reaction enthalpies were taken from NIST-JANAF thermochemical tables [3].

We can assume that H_2, H_2O, and CH_4 are well-described by PBE and thus use them without correction as they are singly-bonded and the earlier error analysis shows these are not strongly affected by DFT errors [2]. Then, using the following three reactions and their corresponding reaction enthalpies, errors for O_2, CO and CO_2, respectively, can be evaluated:

$$2\,\mathrm{H_2O\,(g)} \longrightarrow \mathrm{O_2\,(g)} + 2\,\mathrm{H_2\,(g)}; \tag{S3}$$

$$\mathrm{CH_4\,(g)} + \mathrm{H_2O\,(g)} \longrightarrow \mathrm{CO\,(g)} + 3\,\mathrm{H_2\,(g)}; \tag{S4}$$

$$\mathrm{CH_4\,(g)} + 2\,\mathrm{H_2O\,(g)} \longrightarrow \mathrm{CO_2\,(g)} + 4\,\mathrm{H_2\,(g)}. \tag{S5}$$

This method results in the error correction terms $\varepsilon_{\mathrm{O_2}} = 0.65\,\mathrm{eV}$, $\varepsilon_{\mathrm{CO}} = -0.32\,\mathrm{eV}$, and $\varepsilon_{\mathrm{CO_2}} = 0.17\,\mathrm{eV}$. The magnitudes of these errors are similar to those obtained in a number of other works investigating DFT error correction [2, 4, 5].

S2 Global minimum structures

The global minimum structures of Zn_yO_x/Cu(111), In_yO_x/Cu(111), and In_yO_x/Pd(111) nanoclusters are highlighted in the main text (Figures 2 to 4). The global minimum structures of the other three explored systems (Zn_yO_x/Pd(111), Zn_yO_x/Au(111), and In_yO_x/Au(111)) are shown below in Figures S1 to S3.

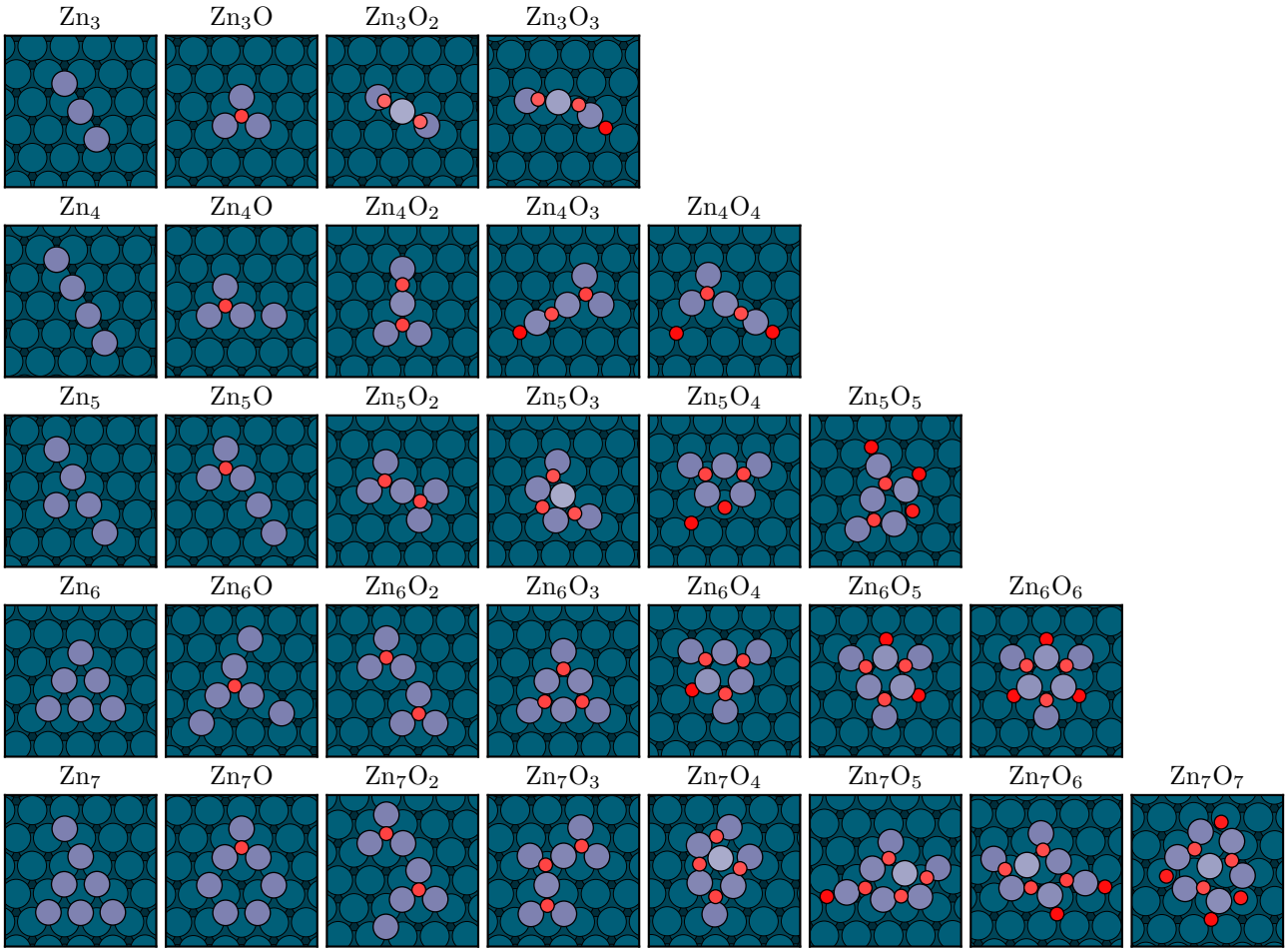

Figure S1: **Global minimum energy structures of Zn_yO_x/Pd(111) nanoclusters with $3 \leq y \leq 7$ and $0 \leq x \leq y$.** Top-down views of the structures. The lightness of colors indicates z coordinate value; lighter atoms have a higher z coordinate.

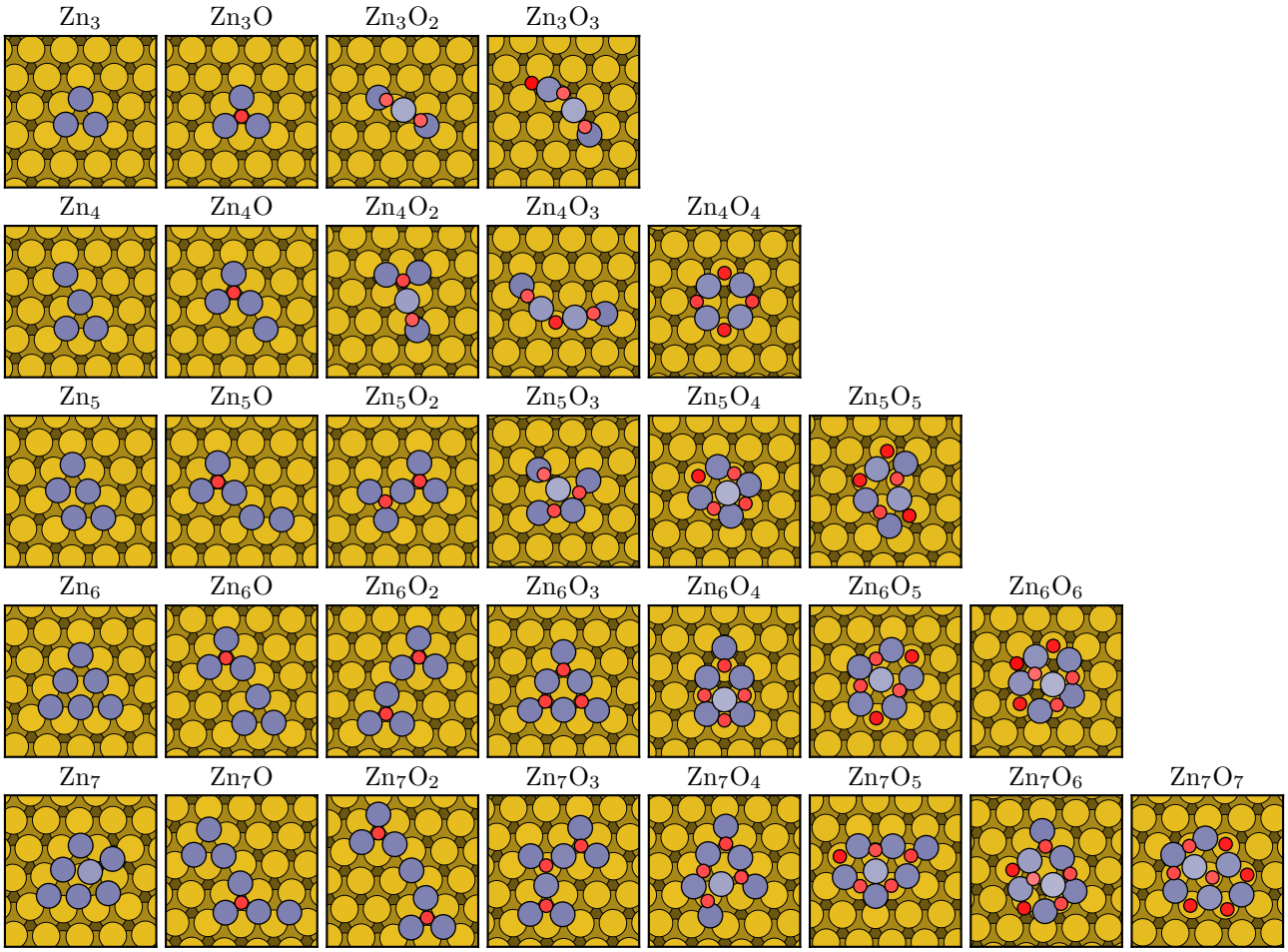

Figure S2: **Global minimum energy structures of Zn_yO_x/Au(111) nanoclusters with $3 \leq y \leq 7$ and $0 \leq x \leq y$.** Top-down views of the structures. The lightness of colors indicates z coordinate value; lighter atoms have a higher z coordinate.

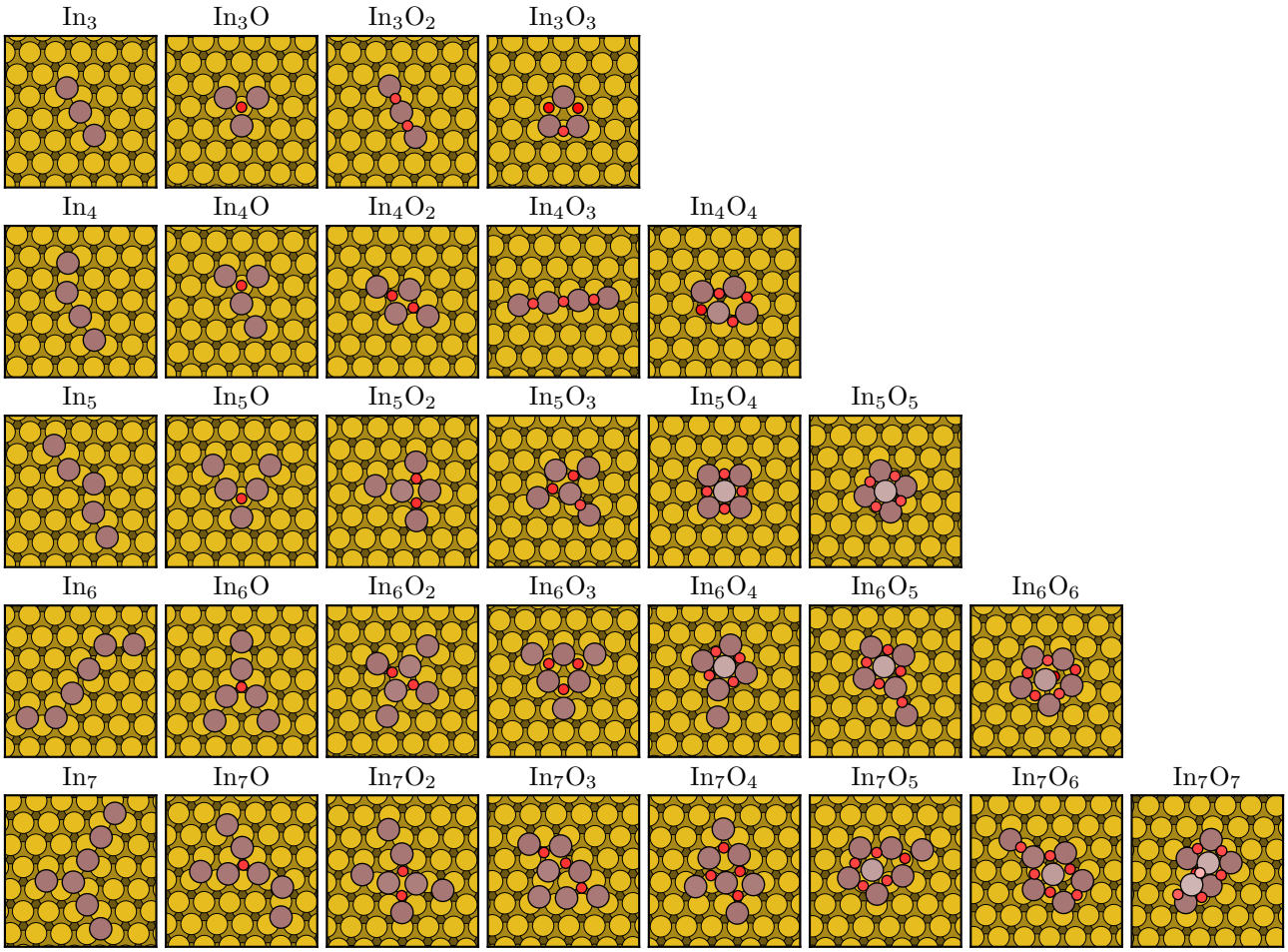

Figure S3: **Global minimum energy structures of In_yO_x/Au(111) nanoclusters with $3 \leq y \leq 7$ and $0 \leq x \leq y$.** Top-down views of the structures. The lightness of colors indicates z coordinate value; lighter atoms have a higher z coordinate.

S3 *Ab initio* thermodynamics

S3.1 Free energy diagrams

The free energy diagram of Zn_yO_x/Cu(111) is highlighted in the main text (Figure 6). The free energy diagrams (including Gibbs free energies) of the other five explored systems are shown below in Figures S4 to S8.

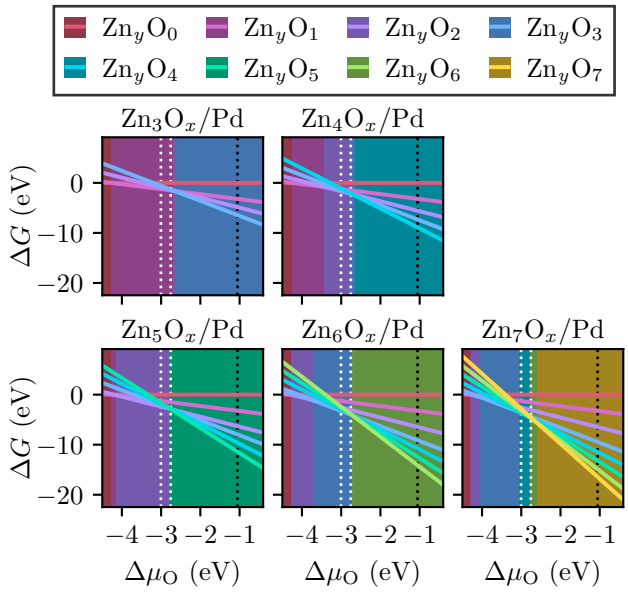

Figure S4: **Gibbs free energies of Zn_yO_x/Pd(111) nanoclusters in equilibrium with an oxygen environment.** A detailed description is given in the caption of Figure 6.

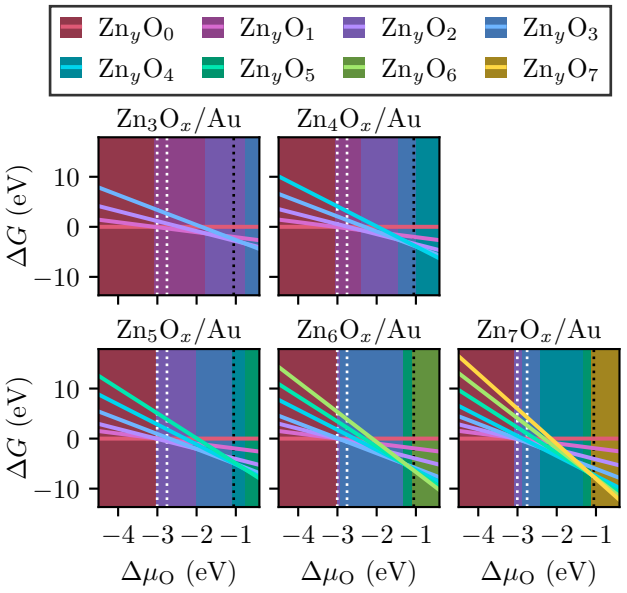

Figure S5: **Gibbs free energies of Zn_yO_x/Au(111) nanoclusters in equilibrium with an oxygen environment.** A detailed description is given in the caption of Figure 6.

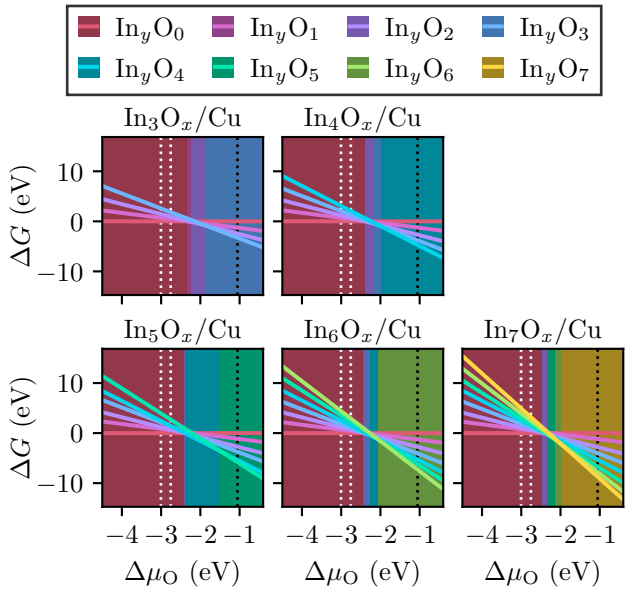

Figure S6: **Gibbs free energies of In_yO_x/Cu(111) nanoclusters in equilibrium with an oxygen environment.** A detailed description is given in the caption of Figure 6.

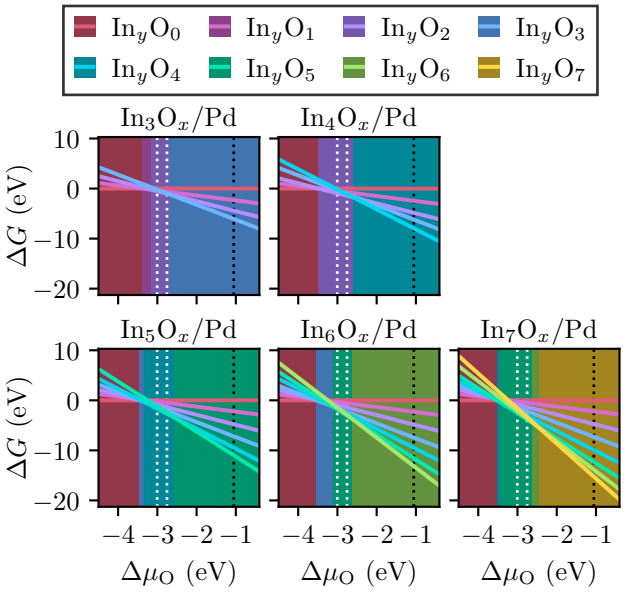

Figure S7: **Gibbs free energies of In_yO_x/Pd(111) nanoclusters in equilibrium with an oxygen environment.** A detailed description is given in the caption of Figure 6.

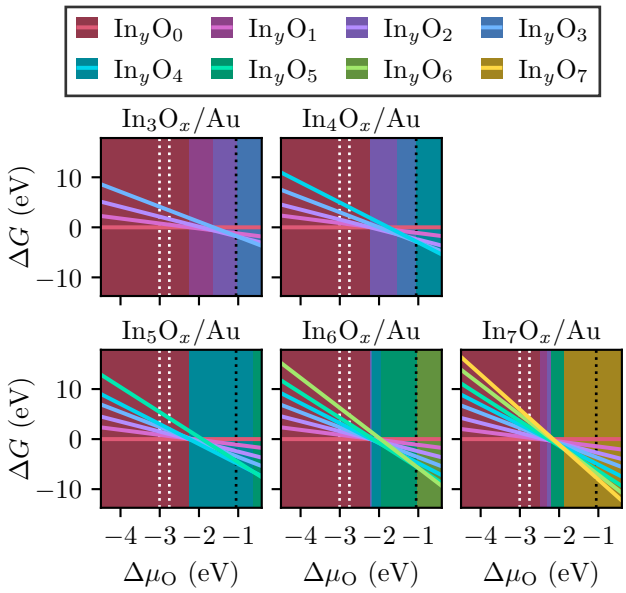

Figure S8: **Gibbs free energies of In_yO_x/Au(111) nanoclusters in equilibrium with an oxygen environment.** A detailed description is given in the caption of Figure 6.

S3.2 Single-atom alloys

As a model for surface alloys, we created single-atom alloy geometries by replacing one surface metal atom in the 7×7 slab with the alloyed metal. Under the assumption that the surface atom removed to form the alloy has a Gibbs free energy equivalent to a bulk metal atom, the Gibbs free energy differences between the single-atom alloy systems and the pure-metal nanoclusters were determined. Table S1 shows these Gibbs free energy differences normalized for the number of atoms, where the pure-metal nanocluster is used as a reference; thus, negative values indicate that the single-atom alloy is more stable.

Using *ab initio* thermodynamics, the stability of these single-atom alloys can also be related to that of oxidized nanoclusters in an oxygen-containing environment, as shown in Figure 8 in the main text.

Table S1: Difference between Gibbs free energy of pure-metal nanoclusters and that of the single-atom surface alloy, in eV atom^{-1}.

	Nanocluster system					
y	Zn_y/Cu(111)	Zn_y/Pd(111)	Zn_y/Au(111)	In_y/Cu(111)	In_y/Pd(111)	In_y/Au(111)
3	−0.44	−0.75	−0.45	−0.38	−0.84	−0.54
4	−0.41	−0.74	−0.46	−0.40	−0.85	−0.54
5	−0.40	−0.75	−0.45	−0.38	−0.85	−0.57
6	−0.38	−0.74	−0.44	−0.37	−0.86	−0.56
7	−0.38	−0.74	−0.45	−0.37	−0.86	−0.58

S3.3 Hydroxylated nanoclusters

For five Zn_5O_x/Cu(111) and Zn_6O_x/Cu(111) structures, stable across a reasonable range of reaction conditions, we created hydroxylated geometries. This was done by placing hydrogen atoms near all oxygen atoms of these structures and relaxing the structures using the same protocol as applied to all other structures. This resulted in the five hydroxylated nanoclusters $Zn_5O_2H_2$, $Zn_5O_5H_5$, $Zn_6O_2H_2$, $Zn_6O_3H_3$, and $Zn_6O_6H_6$, all supported by the Cu(111) surface. The oxidized and hydroxylated nanocluster geometries are shown in Figure S9.

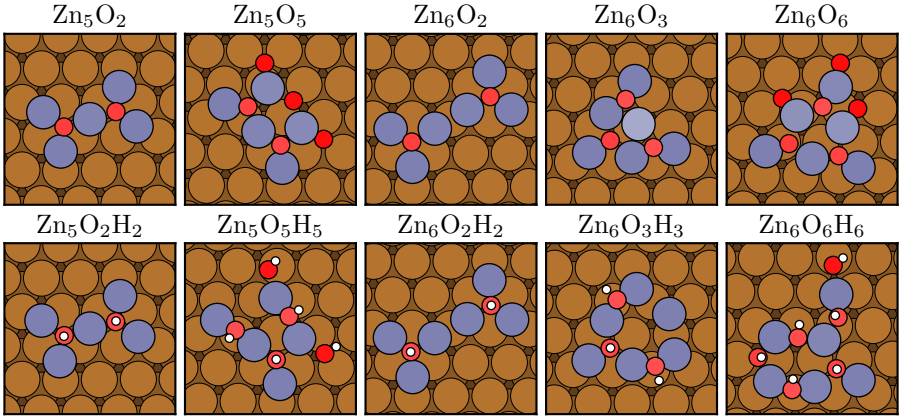

Figure S9: **Oxidized and hydroxylated nanoclusters.** A subset of Zn_yO_x/Cu(111) global minimum structures obtained using the workflow in this work (top row) and hydroxylated $Zn_yO_xH_x$/Cu(111) structures obtained by adding hydrogen atoms near all oxygen atoms of the corresponding Zn_yO_x/Cu(111) structures and relaxing these structures into their local minima (bottom row).

Using the hydroxylated structures shown in Figure S9 and all other Zn_yO_x/Cu(111) structures, a two-dimensional phase diagram was created, shown in Figure S10. To create this phase diagram, the oxygen and hydrogen reservoirs were assumed to be independent, such that the most thermodynamically stable structure can be described as a function of both $\Delta\mu_O$ and $\Delta\mu_H$. Using the *ab initio* thermodynamics approach outlined in Section 3.5, we can define the hydrogen chemical potential as $\mu_H = \frac{1}{2}\mu_{H_2}$, which, when used in combination with the typical methanol synthesis reaction conditions, results in the range

$$-0.30\,\text{eV} < \Delta\mu_H < -0.19\,\text{eV}. \tag{S6}$$

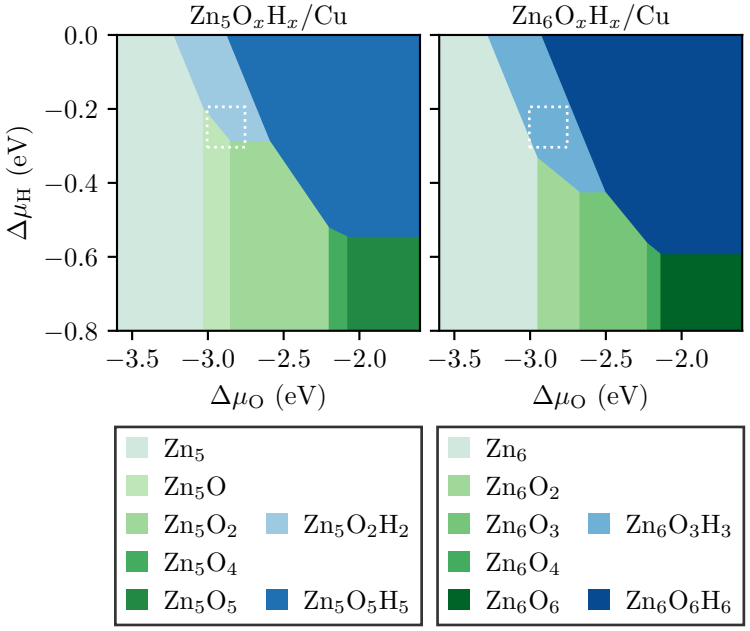

Figure S10: **Most thermodynamically stable composition of all evaluated Zn_5O_x/Cu(111) and Zn_6O_x/Cu(111) systems and selected hydroxylated clusters in equilibrium with an environment containing independent oxygen and hydrogen reservoirs.** Based on the global minimum structures found for Zn_yO_x/Cu(111) (Figure 2) and the structures shown in Figure S9. The region highlighted with white dotted lines corresponds to typical methanol synthesis conditions as given in Equations (S6) and (11).

References

1. Christensen, R., Hansen, H. A. & Vegge, T. Identifying systematic DFT errors in catalytic reactions. *Catalysis Science & Technology* **5,** 4946–4949. ISSN: 2044-4761. http://dx.doi.org/10.1039/c5cy01332a (2015).
2. Cheula, R. & Maestri, M. Nature and identity of the active site via structure-dependent microkinetic modeling: An application to WGS and reverse WGS reactions on Rh. *Catalysis Today* **387,** 159–171. ISSN: 0920-5861. http://dx.doi.org/10.1016/j.cattod.2021.05.016 (2022).
3. Chase, M. W. *NIST-JANAF Thermochemical Tables* 4th ed. https://janaf.nist.gov/ (American Institute of Physics, 1998).
4. Granda-Marulanda, L. P. *et al.* A Semiempirical Method to Detect and Correct DFT-Based Gas-Phase Errors and Its Application in Electrocatalysis. *ACS Catalysis* **10,** 6900–6907. ISSN: 2155-5435. http://dx.doi.org/10.1021/acscatal.0c01075 (2020).
5. Sargeant, E., Illas, F., Rodríguez, P. & Calle-Vallejo, F. Importance of the gas-phase error correction for O_2 when using DFT to model the oxygen reduction and evolution reactions. *Journal of Electroanalytical Chemistry* **896,** 115178. ISSN: 1572-6657. http://dx.doi.org/10.1016/j.jelechem.2021.115178 (2021).